The Astronomical Journal, 170:284 (8pp), 2025 November https://doi.org/10.3847/1538-3881/ae0a2b

On the Detection of Exorings in Reflected Light with JWST NIRCam

Rachel Bowens-Rubin[1,2], Mary Anne Limbach[1], Sam Hopper[1], Klaus Subbotina Stephenson[3,4], Matson Garza[5], Leigh N. Fletcher[6], and Matthew Hedman[7]
[1] Department of Astronomy, University of Michigan, Ann Arbor, MI 48109, USA; rbowens-rubin@mit.edu
[2] Eureka Scientific Inc., 2542 Delmar Avenue, Suite 100, Oakland, CA 94602, USA
[3] Department of Physics and Astronomy, University of Victoria, 3800 Finnerty Road, Elliot Building, Room 207, Victoria, BC V8P 5C2, Canada
[4] Department of Astronomy & Astrophysics, University of California, Santa Cruz, 1156 High Street, Santa Cruz, CA 95064, USA
[5] Department of Physics, Massachusetts Institute of Technology, 77 Massachusetts Avenue, Cambridge, MA 02139, USA
[6] School of Physics and Astronomy, University of Leicester, University Road, Leicester LE1 7RH, UK
[7] Department of Physics, 875 Perimeter Drive MS 0903, Moscow, ID 83844, USA
Received 2025 July 11; revised 2025 August 28; accepted 2025 August 29; published 2025 October 27

Abstract

When directly imaging a cold-giant exoplanet hosting a ring system, the reflected light from the rings can outshine the planet's thermal emission and reflected light in the near-infrared. Consequently, an exoring may be detectable at a significantly lower contrasts than is required to image the exoplanet itself. Here we investigate the detectability of exorings in near-infrared reflected light using NIRCam coronagraphy `PanCAKE` simulations of two nearby mature stars, Proxima Centauri and Tau Ceti. Under the most favorable assumptions, we find JWST 2 μm NIRCam coronagraphy (F200W + MASK335R) is capable of detecting an exoring system with a radius of 2.8 times that of Saturn's A-ring for planets on an orbit with $a = 1.3$–1.9 au. Broader simulations indicate that NIRCam can probe large planetary ring systems around mature exoplanets comparable in size to circumplanetary disks, which can reach up to 1000 times the radius of Saturn's A-ring. These results suggest that NIRCam F200W coronagraphy could serendipitously detect large exorings in reflected light under the right conditions. A combined analysis of F200W coronagraphic observations of confirmed exoplanets could provide the first empirical constraints on the occurrence rate of large exorings. Confirming the existence and frequency of exorings spanning the scale between circumplanetary disks and the rings of the solar system giant planet could offer new insight into the formation, evolution, and architecture of planetary systems.

Unified Astronomy Thesaurus concepts: Direct imaging (387); Exoplanet rings (494); James Webb Space Telescope (2291)

1. Introduction

Ringed exoplanets offer a unique opportunity to study planetary formation, dynamical evolution, and system architectures. Several theoretical and observational studies propose mechanisms by which rings may form around exoplanets, including collisions between minor bodies (R. Hyodo & K. Ohtsuki 2015), tidal disruption or stripping of a minor body (R. M. Canup 2010; J. Wisdom et al. 2022), the incomplete dissipation of a primordial circumplanetary disk (W. F. Bottke et al. 2005), and material ejection from an active moon (B. A. Smith et al. 1979). One of the major open questions about Saturn concerns the age of its rings and the rate to which they are replenished. Understanding the census of planetary rings beyond the solar system could provide valuable constraints on these processes for a diversity of worlds, improve our understanding of planetary system demographics, and place the frequency of ringed exoplanets in the broader context.

The presence of a ring system can significantly affect the observable properties of an exoplanet, influencing their inferred radii, densities, and albedos (J. W. Barnes & J. J. Fortney 2004; L. Arnold & J. Schneider 2006). For example, the anomalously large radii of the so-called "super-puff" planets HIP 41378 f and Kepler 90 g relative to their masses have been hypothesized to result from the presence of extended ring systems (B. Akinsanmi et al. 2020; Y. Liang et al. 2021; T. Lu et al. 2025). A number of other exoplanets with well-characterized mass and radius measurements also fall into the superpuff category (A. L. Piro & S. Vissapragada 2020). If rings are indeed responsible for the observed low densities of these planets, this would imply that ringed exoplanets may be somewhat common, particularly given the significant number of long-period transiting planets with measured masses that appear underdense.

In addition to influencing bulk properties, rings can also affect a planet's atmospheric composition and thermal structure. The material from the rings may fall onto the planet, delivering exogenic species such as oxygen-bearing compounds to the upper atmosphere. This influx can initiate photochemical reactions involving oxygen and carbon, as observed in Saturn's atmosphere from Cassini data (J. H. Waite et al. 2018). Ring particles may also follow magnetic field lines and deposit in specific regions, altering the ionospheric composition at midlatitudes through localized "ring rain" (J. O'Donoghue et al. 2016). Furthermore, rings can cast shadows on the planetary atmosphere, creating temperature gradients and localized cooling in the stratosphere. These shadowing effects have been shown to influence atmospheric dynamics on Saturn, leading to banded temperature structures and circulation patterns that redistribute heat (L. N. Fletcher et al. 2018). Together, these processes demonstrate that rings may alter not only how exoplanets appear in observations but also their atmospheric chemistry and climate.

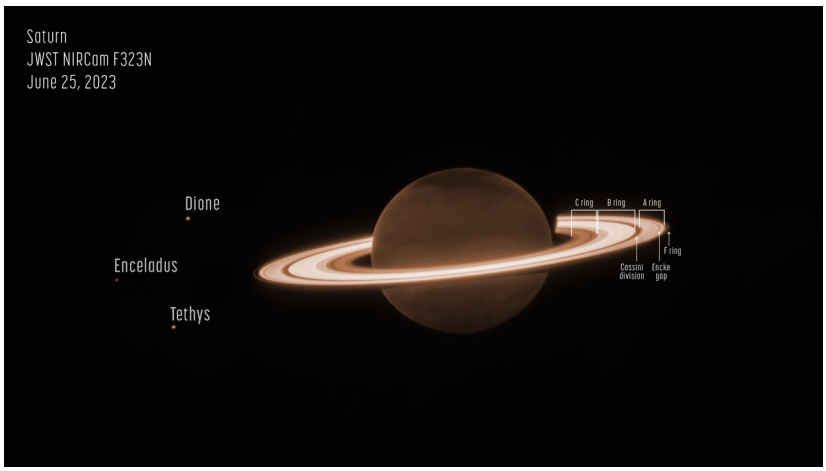

(a) Saturn NIRCam F323N

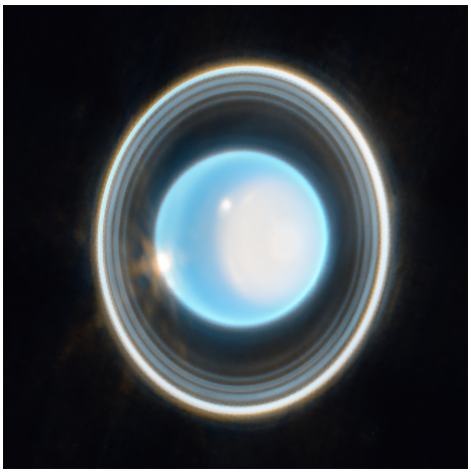

(b)Uranus NIRCam F140M (Cyan) & F300M (Orange) Composite

Figure 1. The rings of Saturn and Uranus as imaged by JWST NIRCam. These images provide an empirical example in which the flux of the ring system is comparable to, or even exceeds, that of the planet when observed with NIRCam. The image of Saturn was created using data from JWST GTO 1247. (a) (GTO 1247: https://www.stsci.edu/jwst/science-execution/program-information?id=1247; image credit: NASA, ESA, CSA, Matthew Tiscareno (SETI Institute), Matthew Hedman (University of Idaho), Maryame El Moutamid (Cornell University), Mark Showalter (SETI Institute), Leigh Fletcher (University of Leicester), Heidi Hammel (AURA)). (b) The image of Uranus was created using data from JWST DD 2739. (DD 2739: https://www.stsci.edu/jwst-program-info/program/?program=2739; image credit: Joseph DePasquale (STScI); NASA, ESA, CSA, STScI).

While an exoring system around a mature exoplanet has yet been conclusively confirmed, circumplanetary disks around young accreting exoplanets have been observed. Direct-imaging detections of circumplanetary disks have been reported in several systems, including J1407b (M. A. Kenworthy & E. E. Mamajek 2015), PDS 70 c (M. Benisty et al. 2021), AS 209 (J. Bae et al. 2022), HD 100546b (S. P. Quanz et al. 2013), and YSES-1b (K. Hoch et al. 2025). While circumplanetary disks trace the initial conditions of material accreting onto forming giant planets and the early stages of satellite formation (R. M. Canup & W. R. Ward 2002; W. F. Bottke et al. 2005; J. Szulágyi et al. 2018), exorings detected around mature planets can offer similar insight into the dynamical evolution of planetary systems, including tidal interactions, satellite disruption, or migration-driven instabilities that reshape or destroy moon systems over time (R. M. Canup 2010; A. J. Hesselbrock & D. A. Minton 2019).

In reflected-light direct imaging, planetary rings can contribute significantly to the total brightness of a system. Because they can have a larger surface area and higher albedo than the planet, rings may outshine the planet itself under certain viewing geometries. In the solar system, all four giant planets are known to host rings (J. L. Elliot et al. 1977; W. B. Hubbard et al. 1986; B. A. Smith et al. 1989), with Saturn's system being the most prominent. At near-infrared wavelengths, particularly where methane absorption bands reduce the planet's flux, Saturn's rings can appear nearly 100 times brighter than the planet. This effect is evident in recent JWST/NIRCam narrowband imaging of Saturn with the F323N filter (see Figure 1). Similar behavior is observed in medium-band NIRCam filters, where the rings of both Saturn and Uranus can appear as bright or brighter than the planets themselves (M. M. Hedman et al. 2025).

Due to the high reflectivity of icy rings, the contrasts needed to detect exorings in reflected light can be orders of magnitude less than what would be required for reflected light or thermal emission imaging of mature (cold) giant planets. Moreover, targeting the light reflected off a planetary ring system may open the discovery space toward finding mature sub-Jupiter mass exoplanets that would otherwise be too cold/small/nonreflective to be directly detected by imaging.

These characteristics raise a compelling question: could rings around cold/mature exoplanets in the nearest systems be detectable in reflected light with JWST NIRCam coronagraphy (M. D. Perrin et al. 2018; J. H. Girard et al. 2022)? In this work, we explore such a possible search by simulating the contrast of JWST NIRCam for two nearby systems and applying simplified ring models. In Section 2, we describe our methods for simulating the JWST contrast and understanding these contrast measurements with respect to ring-radius constraints. In Section 3, we show the results of simulating the Proxima Centauri and Tau Ceti systems. Section 4 presents our findings and explores future prospects for exoring detection, while Section 5 provides a summary of our results.

2. Methods

2.1. Simulating JWST NIRCam Coronagraphy Contrast

We present simulations of two example cases of mature, nearby systems with different stellar types: Proxima Centauri and Tau Ceti. Proxima Centauri is an M5.5V star (M. S. Bessell 1991) of age 4.85 Gyr (P. Kervella et al. 2003) at a distance of 1.3 pc (Gaia Collaboration et al. 2021). Tau Ceti is a G8V star (P. C. Keenan & R. C. McNeil 1989) with an age of 8–10 Gyr (Y. K. Tang & N. Gai 2011) at 3.7 pc (Gaia Collaboration et al. 2021). Both of these systems have multiple confirmed exoplanets or candidates that have been identified through radial velocity (X. Dumusque et al. 2012; G. Anglada-Escudé et al. 2016; F. Feng et al. 2017; M. Damasso et al. 2020; J. P. Faria et al. 2022).

We simulated the NIRCam coronagraphy contrast performance using the Pandeia Coronagraphy Advanced Kit for Extractions (`PanCAKE`) python package[8] (J. H. Girard et al.

[8] Pandeia Coronagraphy Advanced Kit for Extractions: https://github.com/spacetelescope/pandeia-coronagraphy.

2018, M. D. Perrin et al. 2018, A. L. Carter et al. 2021). In order to represent a case for a feasible future observation of a nearby bright star, we replicated the observing configurations for previously performed NIRCam coronagraphy observations of nearby bright stars. For Proxima Centauri, we replicated the NIRCam configuration used to observe the nearby M-dwarf systems in the GO 6122 program in F200W/F444W (R. Bowens-Rubin et al. 2024): SUB320/MEDIUM8 readout, eight groups/int, 36 int/exp, and 3041s total time. For Tau Ceti, we replicated the NIRCam configuration used to perform an observation of Fomalhaut in F356W in the GO 1193 program (C. A. Beichman et al. 2017; M. Ygouf et al. 2024): SUB320/RAPID readout, three groups/int, 105 ints/exp, and 451 s total time.

We simulated the NIRCam coronagraphy observations of Proxima Centauri and Tau Ceti using all the combinations of masks and filters available in `PanCAKE`. Five masks were simulated: MASK210R, MASK335R, MASK430R, MASKLWB, and MASKSWB. The following filters were simulated in combination with their allowed masks: F164N, F182M, F187N, F200W, F210M, F212N, F250M, F277W, F300M, F322W2, F323N, F335M, F356W, F360M, F405N, F410M, F430M, F444W, F460M, F466N, F470N, F480M.

The coronagraphs available with NIRCam cannot operate at shorter wavelengths ($<1.64\,\mu$m) because the optical wedges that project the occulting masks onto the detectors introduce chromatic aberrations, and the antireflective coating on the coronagraph substrate exhibits poor throughput in this regime. This limitation is unfortunate, as shorter wavelengths are likely optimal for detecting exorings in reflected light.

We modeled the PSF subtraction as angular differential imaging (ADI) and reference differential imaging with a five-point-diamond dither on the reference star and a roll angle of 10°. We assumed a perfect reference star match by inputting the target star properties as the reference star, following the steps of the `PanCAKE` basic tutorial.[9] Due to the internal limits of the `PanCAKE` software, the contrast limits were only simulated out to a separation of 1.″46. However, the field of view of the SUB320 array is 10″ in the short wavelength filters,[10] so we estimated the contrasts to a 5″ radius by extrapolating using a linear fit of the final 3 points of the `PanCAKE` simulation. This extrapolation represents a pessimistic scenario, as if the best background limit was achieved by 1.″46. However, on-sky results have shown that improved background limits can be achieved beyond 1.″5 of separation (see NIRCam F444W+MASK335R contrast curves in A. L. Carter et al. 2023 and R. Bowens-Rubin et al. 2025 examples, which reach the best background limits beyond 2.″5).

We do not consider the use of NIRCam's direct imaging mode (no coronagraph) in this study, as the instrument generally saturates at the small angular separations corresponding to the projected locations of the optimal location for observing ring systems around nearby stars. This saturation renders observations of exorings infeasible at the spatial scales of interest. We focus this analysis on NIRCam's coronagraphic mode only.

[9] The `PanCAKE` tutorial referenced here can be accessed at https://aarynncarter.com/PanCAKE/notebooks/pancake_basic_tutorial.html.

[10] Field of view of the SUB320 array with MASK335R is listed in Table 2 of the JDocs accessed at https://jwst-docs.stsci.edu/jwst-near-infrared-camera/nircam-instrumentation/nircam-detector-overview/nircam-detector-subarrays.

2.2. Converting Simulated Contrast to Ring Size Estimates

The primary observational limitation in detecting reflected light from planetary rings is the contrast between the rings and the host star. The reflected flux scales proportionally with the incident stellar flux, thus the detectability of planetary rings is independent of the type of star the planet orbits. Ring systems have lower (more favorable) ring-to-star contrasts when they are closer to their star, larger in area, highly reflective, and in an optimal geometric configuration to reflect light at the observer.

To examine the set of possible exoplanet ring systems that could be detectable from our simulated contrast curves, we adopted the following assumptions:

1. The ring is observed in a face-on configuration, reflecting the maximum amount of light toward the observer.
2. The rings do not contribute flux from thermal emission; all detected flux arises from stellar light reflected by the ring.
3. The optical depth of the ring is high throughout the full area of the ring .
4. The thermal emission and reflected light from the planet contributes negligibly to the total flux compared to the reflected light from the ring.

We considered two cases for the ring's reflectivity:

1. Fully reflective ring (ring particles have albedo = 1 and ring is opaque): this idealized scenario represents the maximum possible reflectance and is broadly applicable to the visible and near-infrared if the ring is composed primarily of water ice with specific grain sizes. For example, 1 μm-sized grains can yield an albedo of ∼0.95 over the 0.2–2 μm range (see Figure 4 of R. N. Clark et al. 2019).
2. Saturn-like ring reflectivity (ring particles have albedo = 0.36 and ring is opaque): Figure 2 shows the reflectance spectrum and albedo of Saturn's rings overlaid with the transmission curves of JWST/NIRCam wideband filters. We adopted the reflectivity of Saturn's B ring expected in the F200W filter in this case (albedo = 0.36; M. Ciarniello et al. 2019).

Under these assumptions, the observed contrast between the planetary ring system and the host star is given by

$$\text{contrast} = \frac{\text{albedo} * \pi(R_{\text{out}}^2 - R_{\text{in}}^2)}{4\pi d^2}, \quad (1)$$

where $R_{\text{in}}/R_{\text{out}}$ are the inner/outer radii of the ring and d is the projected star-to-planet/ring orbital separation.

When referring to the area of Saturn's rings in this work, we use a reference value corresponding to the inner edge of Saturn's D ring of $R_{\text{in}} = 66{,}900$ km (C. D. Murray & S. F. Dermott 1999; R. G. French et al. 2017) and the outer edge of Saturn's A ring of $R_{\text{out}} = 136{,}780$ km (M. El Moutamid et al. 2016). In later sections, we vary the size of the rings discussed by changing the value of the outer ring radius.

2.3. Limit to the Outer Radius of an Exoring

Saturn has the largest ring system in our solar system, yet there are virtually no observational constraints on how large an exoring system could be. As a theoretical upper limit, one can

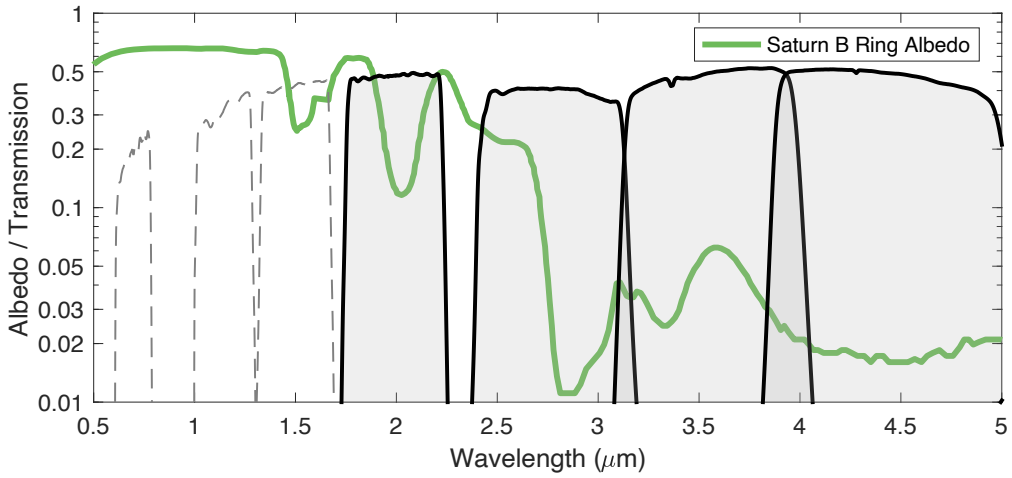

Figure 2. The albedo spectrum of Saturn's B-ring across the visible and near-infrared. The measurement of the albedo of Saturn's rings *(green)* is plotted alongside the wavelength ranges of the JWST NIRCam wideband filters. The filters unavailable for coronagraphy (F070W, F115W, F150W) are shown in dotted lines. The filters availble for coronagraphy (F200W, F277W, F356W and F444W) are plotted with the thick black lines and gray shading. Saturn's rings show a reasonably high reflectivity at $\lesssim$2 μm but drop significantly at longer wavelengths.

assume that a ring system could extend as far as the planet's Hill sphere. The Hill radius ($R_{\rm H}$) increases with planetary mass (m_2), orbital distance (a), and decreases with stellar mass (m_1), following:

$$R_{\rm H} \approx a(1-e)\left(\frac{m_2}{3(m_1+m_2)}\right)^{1/3}. \quad (2)$$

For a Sun–Saturn analog system, the Hill radius extends to $R_{\rm out} = 0.44$ AU (6.5×10^7 km), more than 470 times the outer radius of Saturn's A ring. For the mature super-Jupiter exoplanet Eps Indi Ab, the Hill radius is 2.3 au (3.4×10^8 km), roughly 2515 times larger than Saturn's A ring.

Although exorings have yet to be detected in these older systems, circumplanetary disks observed around young planets exhibit radii comparable to these theoretical maxima. For example, the disk around PDS 70 c spans ~1.2 au which is near its Hill radius (M. Benisty et al. 2021). The disk surrounding J1407b has an estimated radius of up to 0.6 au (9×10^7 km), approximately 0.15 of its Hill radius (200× the radius of Saturn's ring system; T. I. M. van Werkhoven et al. 2014).

While it may be possible for a high-opacity distribution of dust or ice grains to extend out to a significant portion of the Hill sphere, the planetary ring systems found around the solar system giant planets contain regions of high and low optical depth. The most opaque rings lie closer to the Roche limit, the distance within which tidal forces from the planet prevent moons from existing. Distances a few times that of the Roche limit may then serve as a more empirically motivated boundary for the outer extent of exoring structures that would be of high enough opacity to be detectable. For Eps Indi Ab, the Roche limit is roughly 3.5×10^5 km (2.6× Saturn's A-ring radius) for a moon that is a fluid-body with the density of water ice.[11]

Although we lack strong examples of planetary ring systems extending far beyond the Roche limit in our own solar system, the diversity of planetary architectures revealed by exoplanet surveys suggests that even extreme configurations should not be dismissed without observational evidence. To date, the transition from young circumplanetary disks to mature ring systems remains largely unexplored and the occurrence rates of such exoring systems have yet to be measured.

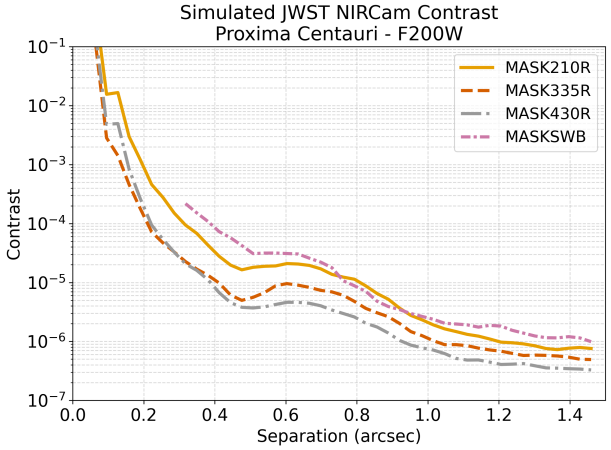

Figure 3. NIRCam Contrast Simulations To Determine the Optimal Mask. An example of the `PanCAKE` contrast simulations are shown for Proxima Centauri with the F200W filter. This example is consistent across both targets and other filters. MASK335R and MASK430R are the best performing masks in simulation.

3. Results

Figure 3 shows the results of the PanCAKE sims for Proxima Centauri for the F200W filter. We find that the best performing masks for NIRCam's short wavelength filters are MASK335R and MASK430R. While MASK430R outperforms MASK335R at some separations, we elected to baseline the remainder of the study with MASK335R because of the asymmetry in the field of view of MASK430R at short wavelengths,[12] and MASK335R is currently the mask of choice for the majority of JWST exoplanet direct imaging programs (see GO 4050; A. Carter et al. 2023; GO 5835;

[11] The Eps Indi Ab Roche limit calculation was made assuming the density of Eps Indi Ab was $\rho_{\rm planet} = 6074$ kg m^{-3} and a moon of $\rho_{\rm moon} = 917$ kg m^{-3}.

[12] See jdocs for field of view information: https://jwst-docs.stsci.edu/jwst-near-infrared-camera/nircam-observing-modes/nircam-coronagraphic-imaging.

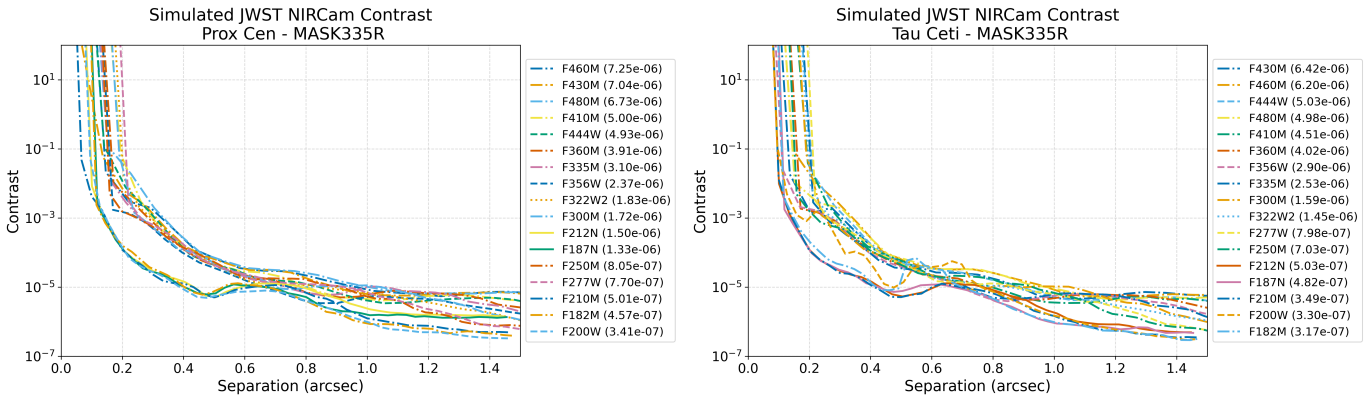

(a) Proxima Centauri (MV5.5; 1.3pc) (b) Tau Ceti (G8V; 3.65pc)

Figure 4. NIRCam coronagraphy simulations with MASK335R to determine the optimal filter. `PanCAKE` was used to simulate the contrast achievable with NIRCam coronagraphy. The contrast predictions for the narrow filters (N) are shown with solid lines, the medium filters (M) are shown in the solid-dot, the wide filters (W) are shown in the dashed–dotted, and the extra wide (W2) are shown in dotted. The values of the simulated contrast at 1.″4 are listed in the legend. The filters are ranked in the order of least to most sensitive. The three filters yielding the best sensitivity for both targets were: F182M, F200W, and F210M.

A. Carter et al. 2024; GO 6012; M. A. Millar-Blanchaer et al. 2024; GO 6122; R. Bowens-Rubin et al. 2024; and SURVEY 6005[13]).

Figure 4 presents the contrast simulations for Proxima Centauri and Tau Ceti for the full set of available filters to perform NIRCam coronagraphy using the MASK335R mask. To determine the optimal filter, we ranked each filter by the contrast value achieved at 1.″4. This separation is within the limits of `PanCAKE` for both the short- and long-wavelength filters and is expected to be near the background-limited regime. The contrast for each filter for Prox Cen and Tau Ceti are listed in the legends of Figure 4.

The three filters that predicted the best contrast performance for Proxima Centauri and Tau Ceti were F182M, F200W, and F210N. The best achievable contrast was 3.4×10^{-7} at 1.″4 (1.8 au) for Proxima Centauri using F200W and 3.2×10^{-7} at 1.″4 (5.1 au) for Tau Ceti using F182N. These filters provide the best JWST contrast performance independently of considering where rings may be most reflective. However, these filters happen to be within the wavelength range where Saturn's B-ring albedo remains reasonably high.

We then converted the simulated F200W contrast curves into estimates of the smallest detectable ring sizes for each system, as shown in Figure 5. These estimates are expressed in terms of the smallest outer ring radius of the exoring system normalized to the outer radius of Saturn's A ring ($R_{\rm out}$ = 136, 780 km). For Proxima Centauri, the minimum detectable ring size for the fully reflective case corresponds to 2.8× the radius of Saturn's rings, with peak sensitivity between 1.3 and 1.9 au (1.″0–1.″5). If the ring reflectivity instead matches that of Saturn's rings (albedo of 0.″36 instead of 1), the detection threshold increases to 4.6 times Saturn's ring radius. In the Tau Ceti system, the minimum detectable ring size under the fully reflective assumption is 6.6 times the radius of Saturn's rings. Assuming Saturn-ring-like reflectivity, this threshold increases to 10.9 times Saturn's ring radius with the optimal sensitivity to planets between 4.0 and 5.3 au (1.″1–1.″5) separation.

[13] SURVEY 6005: https://www.stsci.edu/jwst/science-execution/program-information?id=6005.

Although NIRCam coronagraphy achieves similar contrast performance at a given angular separation in both systems, smaller exorings are detectable around Proxima Centauri than around Tau Ceti due to its closer distance to the observer. Based on Figure 5, we find that ring systems with radii up to 10 times that of Saturn's are potentially detectable around exoplanets at orbital separations of approximately 0.5–10 au in most systems within a few parsecs. However, detectability is limited to a subset of ring properties depending on the ring's reflectivity and viewing inclination. Our results suggest that a planetary ring system with an outer radius of 2.8 times that of Saturn's rings–corresponding to the Proxima Centauri fully reflective case–represents a practical lower size limit for the detectability of reflected light from an exoring system with JWST NIRCam.

4. Discussion

Simulations of JWST NIRCam coronagraphy indicate that while JWST is capable of detecting reflected light from large exoring systems, it cannot detect a ring system comparable in size to Saturn's at any orbital separation–even for the nearest stellar systems. This result aligns with expectations, as JWST was not designed for near-infrared reflected-light imaging of exoplanetary rings.

Nonetheless, the ability to detect ring systems several times larger than Saturn's is a somewhat surprising capability. Observers should keep in mind that if an exoplanet candidate is identified within a suitable separation to receive a sufficient proportion of light from its star and showing a bright excess of flux at F200W as compared to F444W, it may be possible that this excess could be explained by a large-ring system with a similar albedo to Saturn's B-ring (which does not reflect much light in F444W). Many JWST direct imaging programs already include NIRCam F200W coronagraphic imaging as part of their observations, and so it is possible that an accidental detection would be possible for one of these NIRCam surveys. Leveraging archival NIRCam F200W data could provide a first step toward constraining the occurrence rate of giant exoplanetary ring systems. Such an occurrence rate analysis would require care in considering the many degeneracies that could still leave a large-ring systems undetectable to JWST, including misalignment of the rings geometry with respect to

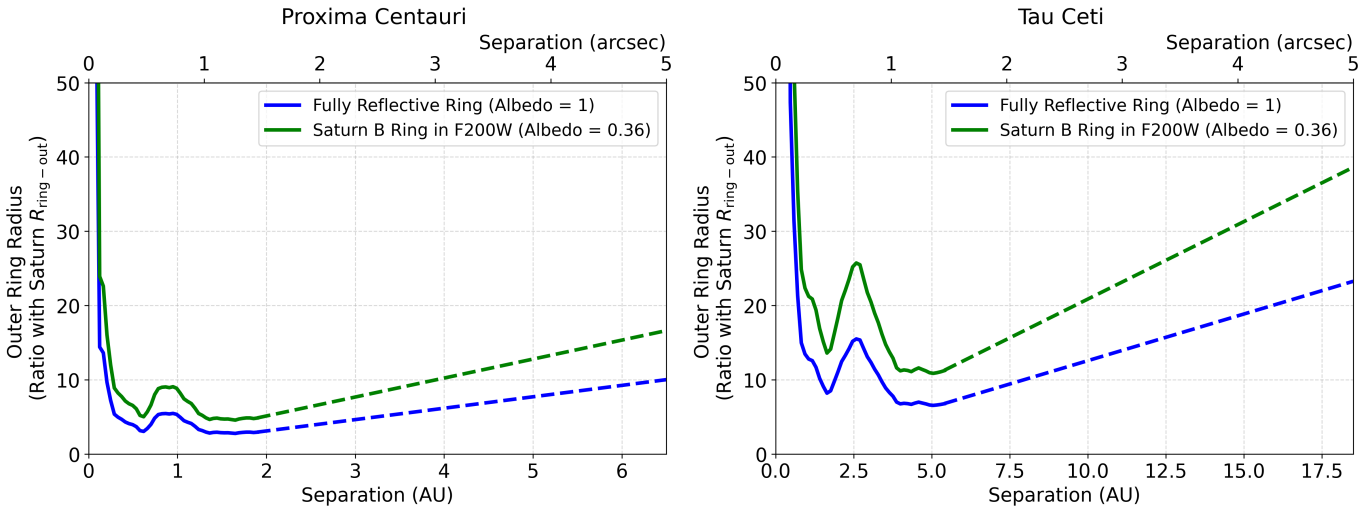

(a) Proxima Centauri (MV5.5; 1.3pc) (b) Tau Ceti (G8V; 3.65pc)

Figure 5. Ring size detectable with JWST. We used the results from the simulations of NIRCam coronagraphy F200W + MASK335R to estimate the smallest ring size detectable for Proxima Centauri and Tau Ceti in the fully reflective case (blue) and the case where the albedo matches that of Saturn's rings at F200W (green). The estimate is shown to the edge of the SUB320 field of view (5″ radius). The dotted lines represent where the contrast was extrapolated linearly from the final three points of the `PanCAKE` simulation. While ring systems smaller than 2.8 the radius of Saturn's rings are not likely to be detectable with JWST through reflected light direct imaging, large-ring systems (tens to thousands of times the size of Saturn's rings) surrounding planets in nearby systems could be possible to detect using NIRCam coronagraphy.

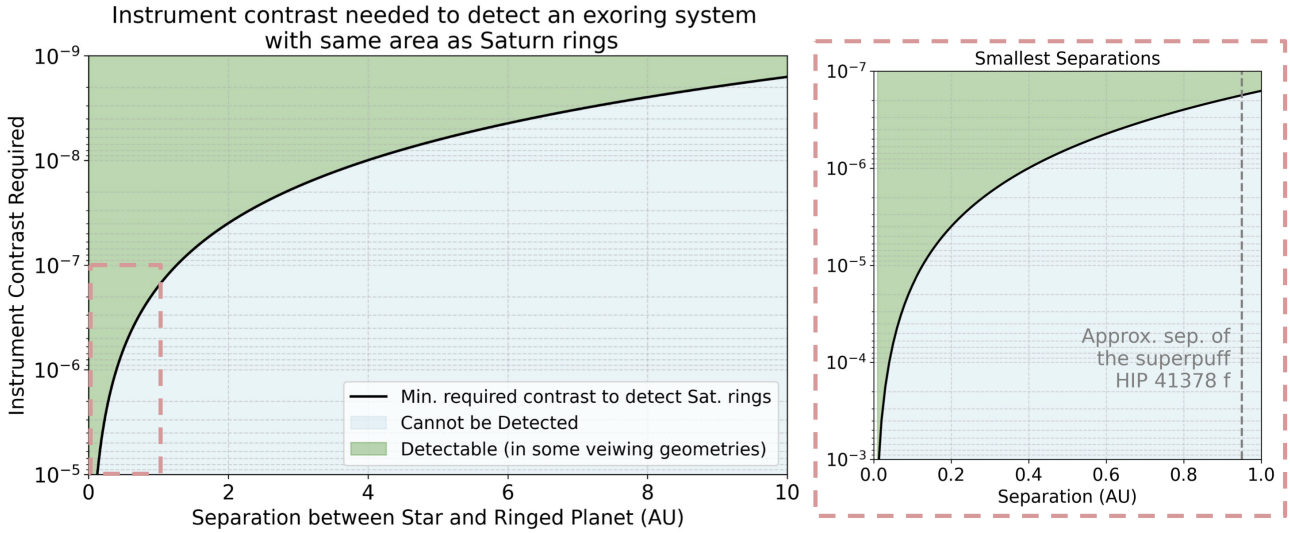

Figure 6. Minimum instrument contrast needed to detect an exoring system with same area as Saturn rings. Instruments capable of reaching contrasts above that of the black line at a given separation (shaded in green) would be capable of detecting face-on, fully reflective exoring systems with the equivalent area of Saturn's rings. As such, the black line provides the most optimistic contrast that would be needed to make the detection. Current ground-based instrumentation may be capable of reaching the contrasts required at tight separations (see zoomed plot on right). (a) The approximate AU separation of the superpuff HIP 41378 f is plotted in gray to show an example of an exoplanet theorized to have a ring system. (The separation of HIP 41378 f was calculated using the central values for the period and the stellar mass provided in A. Vanderburg et al. 2016; while the radius of this ring system is not fully known, the predictions in B. Akinsanmi et al. 2020 indicate that this exoring radius would be likely be smaller than that of Saturn's ring system.) However, large exoring systems are predicted to be rare on tighter orbits due to the gravitational influence of the star. While the contrasts to detect a exoring with the same area as Saturn's rings on orbits outside of 1 au is out of reach for JWST, the contrast performance of future instrumentation is expected to reach this needed sensitivity when directly imaging the nearest-neighboring systems.

the observer, ring systems being made of a nonreflective material, or rings lacking the sufficient grain density to have an opacity to be strongly reflective.

Figure 6 plots the instrument contrast required to discover an exoring system with the equivalent area of Saturn at varying separations from its host star. We again adopt the assumptions outlined in Section 2.2 with the fully reflective case such that this plot represents the minimal instrument contrast that would be required to discover a ring system with the same area as Saturn's rings.

To detect an exoring system the same area as Saturn's around an exoplanet at the same orbital separation as Saturn ($a = 9.58$ au), an instrument contrast of 1.73×10^{-9} or better would be required. This contrast requirement is well within the Habitable Worlds Observatory (HWO) prediction and around the target goal for Nancy Grace Roman Space Telescope

Coronagraph Instrument (Roman CGI; see Figure 16 in K. B. Follette 2023). Because the instrument threshold of detecting small exoring systems will be met with future observatories, considerations must be given for how to disentangle the properties of exoplanets from the properties of exorings when interpreting the flux measurements from a detected source. We are currently exploring the detectability and characterization of exorings with these future observatories in detail in forthcoming work.

The instrument contrast requirements for detecting an exoring with the same area as Saturn's rings becomes more relaxed at smaller separations because of the greater amount of light that reaches the planet at close-in separations. For example, at 1 au an instrumentation contrast of only 1.6×10^{-7} is required in the fully reflective, face-on case. Some ground-based instrumentation may be capable of reaching these contrasts at the required separations when targeting the nearest-neighboring systems. For example, the Gemini Planet Imager was shown to be capable of achieving a contrast of 10^{-7} by $0\farcs7$ (equivalent of 0.9 au if observing Proxima Centauri; K. B. Follette 2023). The Planetary Camera and Spectrograph for the Extremely Large Telescope is expected to reach 10^{-9} at $0\farcs1$ (M. Kasper et al. 2021). However, at particularly small orbital separations, large-ring systems are not expected to persist due to the reduced size of the planet's Hill sphere and increased susceptibility to dynamical perturbations from the nearby host star which can destabilize extended ring structures.

Finally, we briefly examined the relative brightness of Saturn's rings compared to the planet in the mid-infrared (10–25 μm; J. S. D. Blake et al. 2023; L. N. Fletcher et al. 2023; M. M. Hedman et al. 2024). At the wavelengths accessible JWST MIRI, Saturn's thermal emission dominates over flux reflected by its rings. This suggests that studying exorings around cold giant planets with similar temperature (95K) and atmosphere to Saturn will be more favorable at shorter wavelengths where reflected light is more prominent, such as in the NIRCam bandpasses. This advantage stems from the typically higher albedo of icy ring particles. However, the brightness contrast between the rings and planet can vary depending on the composition of both planet and ring. For example, an exoplanet with highly reflective clouds paired with a ring system contaminated with darker material or composed of silicates rather than water ice would display a different trade space. Observations of Saturn demonstrate that at continuum wavelengths its atmospheric reflectivity can be quite high (e.g., Figure 8 of X. Wang et al. 2024), and detailed spectra of both the planet and its rings reveal strong wavelength-dependent behavior (e.g., Figure 10.10 in L. N. Fletcher et al. 2015). These complexities underscore the importance of both wavelength selection and system composition in planning future exoring searches.

5. Conclusions

In this work, we explored the potential of JWST NIRCam coronagraphy to detect reflected light from exoplanetary ring systems. Using the `PanCAKE` Python package, we simulated contrast limits for two nearby, mature star systems. Our key findings are:

1. Among NIRCam coronagraphic modes, the F200W filter paired with the MASK335R provides one of the most favorable configurations for detecting reflected light from exorings.
2. Exoring systems with radii smaller than 2.8 times that of Saturn's rings are unlikely to be detectable via direct imaging with NIRCam coronagraphy at any orbital separation. Consequently, photometric planet characterization using F200W is unlikely to be significantly affected by ring flux unless the rings are substantially larger than those found in our solar system.
3. Rings $\sim$10$\times$ the size of Saturn's are potentially detectable at separations of 0.5–10 au for the closest systems within a few parsecs. This detectability is dependent on the reflectivity of the rings and their viewing geometry.
4. Existing NIRCam F200W coronagraphic observations of nearby stars could be leveraged to constrain the occurrence rate of large exoring systems ($\gtrsim$100$\times$ the size of Saturn's rings). Such constraints represent an important step toward empirically assessing the prevalence of giant exorings around wide-orbit mature exoplanets.

These results demonstrate both the current limitations and potential opportunities for using JWST coronagraphy to detect and constrain the presence of large exoring systems around mature exoplanets. As the JWST NIRCam coronagraphy archival data continues to grow, systematic searches for large exorings may provide an unexpected legacy on the architectures of planetary systems around nearby stars.

Acknowledgments

The authors would like to acknowledge the thousands of people who dedicated themselves to the design, construction, and commissioning of JWST and the current staff at Space Telescope Sciences who operate the telescope. The authors would also like to thank Aarynn Carter and Marshall Perrin for their role in developing and maintaining `PanCAKE`.

Author Contributions

This paper was inspired by the ongoing work by Sam Hopper and Mary Anne Limbach to explore the detectability of exoring systems for HWO and Roman CGI. Sam Hopper's work assembling the literature measurements of the rings of Saturn and considering their observability as an exoring analog led to the natural next questions that were the foundation of this work. Rachel Bowens-Rubin completed the analysis and writing for Sections 2–5 as well as edits to the abstract and Section 1. Mary Anne Limbach authored the initial draft of the abstract and Section 1 and provided edits on the rest of the manuscript. Klaus Subbotina Stephenson provided essential support and guidance for setting up and running the `PanCAKE` simulations. Matson Garza supported the calculations of the Roche limits and Hill sphere values in Section 2.3. Leigh Fletcher and Matthew Hedman provided their expertize regarding planetary ring systems within the solar system to make recommendations and suggestions in the review of early drafts of the manuscript.

Software: `PanCAKE` (J. H. Girard et al. 2018; M. D. Perrin et al. 2018; A. L. Carter et al. 2021), ChatGPT was used to

improve the wording at the sentence level and to assist in coding.

ORCID iDs

Rachel Bowens-Rubin https://orcid.org/0000-0001-5831-9530
Mary Anne Limbach https://orcid.org/0000-0002-9521-9798
Sam Hopper https://orcid.org/0009-0004-6318-6874
Klaus Subbotina Stephenson https://orcid.org/0009-0008-2252-7969
Matson Garza https://orcid.org/0009-0004-7835-3356
Leigh N. Fletcher https://orcid.org/0000-0001-5834-9588
Matthew Hedman https://orcid.org/0000-0002-8592-0812

References

Akinsanmi, B., Santos, N. C., Faria, J. P., et al. 2020, A&A, 635, L8
Anglada-Escudé, G., Amado, P. J., Barnes, J., et al. 2016, Natur, 536, 437
Arnold, L., & Schneider, J. 2006, in IAU Colloq. 200: Direct Imaging of Exoplanets: Science & Techniques, ed. C. Aime & F. Vakili (Cambridge: Cambridge Univ. Press), 105
Bae, J., Teague, R., Andrews, S. M., et al. 2022, ApJL, 934, L20
Barnes, J. W., & Fortney, J. J. 2004, ApJ, 616, 1193
Beichman, C. A., Rieke, G., Bouwman, J., et al. 2017, Cycle #1193,
Benisty, M., Bae, J., Facchini, S., et al. 2021, ApJL, 916, L2
Bessell, M. S. 1991, AJ, 101, 662
Blake, J. S. D., Fletcher, L. N., Orton, G. S., et al. 2023, Icar, 392, 115347
Bottke, W. F., Durda, D. D., Nesvorný, D., et al. 2005, Icar, 175, 111
Bowens-Rubin, R., Limbach, M. A., Carter, A., et al. 2024, Cycle, 3, #6122
Bowens-Rubin, R., Mang, J., Limbach, M. A., et al. 2025, ApJL, 986, L26
Canup, R. M. 2010, Natur, 468, 943
Canup, R. M., & Ward, W. R. 2002, AJ, 124, 3404
Carter, A., Absil, O., Balmer, W., et al. 2024, Cycle, 3, #5835
Carter, A., Balmer, W., Biller, B., et al. 2023, Cycle, 2, #4050
Carter, A. L., Hinkley, S., Kammerer, J., et al. 2023, ApJL, 951, L20
Carter, A. L., Skemer, A. J. I., Danielski, C., et al. 2021, Proc. SPIE, 11823, 118230H
Ciarniello, M., Filacchione, G., D'Aversa, E., et al. 2019, Icar, 317, 242
Clark, R. N., Brown, R. H., Cruikshank, D. P., & Swayze, G. A. 2019, Icar, 321, 791
Damasso, M., Del Sordo, F., Anglada-Escudé, G., et al. 2020, SciA, 6, eaax7467
Dumusque, X., Pepe, F., Lovis, C., et al. 2012, Natur, 491, 207
El Moutamid, M., Nicholson, P. D., French, R. G., et al. 2016, Icar, 279, 125
Elliot, J. L., Dunham, E., & Mink, D. 1977, Natur, 267, 328
Faria, J. P., Suárez Mascareño, A., Figueira, P., et al. 2022, A&A, 658, A115
Feng, F., Tuomi, M., Jones, H. R. A., et al. 2017, AJ, 154, 135
Fletcher, L. N., Greathouse, T. K., Moses, J. I., Guerlet, S., & West, R. A. 2015, arXiv:1510.05690
Fletcher, L. N., King, O. R. T., Harkett, J., et al. 2023, JGRE, 128, e2023JE007924
Fletcher, L. N., Melin, H., Adriani, A., et al. 2018, AJ, 156, 67
Follette, K. B. 2023, PASP, 135, 093001
French, R. G., McGhee-French, C. A., Lonergan, K., et al. 2017, Icar, 290, 14
Gaia Collaboration, Brown, A. G. A., Vallenari, A., et al. 2021, A&A, 649, A1
Girard, J. H., Blair, W., Brooks, B., et al. 2018, Proc. SPIE, 10698, 106983V
Girard, J. H., Leisenring, J., Kammerer, J., et al. 2022, Proc. SPIE, 12180, 121803Q
Hedman, M. M., de Pater, I., Cartwright, R., et al. 2025, PSJ, 6, 204
Hedman, M. M., Tiscareno, M. S., Showalter, M. R., et al. 2024, JGRE, 129, e2023JE008236
Hesselbrock, A. J., & Minton, D. A. 2019, AJ, 157, 30
Hoch, K., Rowland, M., Petrus, S., et al. 2025, AAS Abstracts, 246, 413.03
Hubbard, W. B., Brahic, A., Sicardy, B., et al. 1986, Natur, 319, 636
Hyodo, R., & Ohtsuki, K. 2015, NatGe, 8, 686
Kasper, M., Cerpa Urra, N., Pathak, P., et al. 2021, Msngr, 182, 38
Keenan, P. C., & McNeil, R. C. 1989, ApJS, 71, 245
Kenworthy, M. A., & Mamajek, E. E. 2015, ApJ, 800, 126
Kervella, P., Thévenin, F., Ségransan, D., et al. 2003, A&A, 404, 1087
Liang, Y., Robnik, J., & Seljak, U. 2021, AJ, 161, 202
Lu, T., Li, G., Cassese, B., & Lin, D. N. C. 2025, ApJ, 980, 39
Millar-Blanchaer, M. A., Altinier, L., Carter, A., et al. 2024, Cycle #6012,
Murray, C. D., & Dermott, S. F. 1999, Solar System Dynamics (Cambridge: Cambridge Univ. Press)
O'Donoghue, J., Melin, H., Stallard, T. S., et al. 2016, Icar, 263, 44
Perrin, M. D., Pueyo, L., Van Gorkom, K., et al. 2018, Proc. SPIE, 10698, 1069809
Piro, A. L., & Vissapragada, S. 2020, AJ, 159, 131
Quanz, S. P., Amara, A., Meyer, M. R., et al. 2013, ApJL, 766, L1
Smith, B. A., Soderblom, L. A., Banfield, D., et al. 1989, Sci, 246, 1422
Smith, B. A., Soderblom, L. A., Johnson, T. V., et al. 1979, Sci, 204, 951
Szulágyi, J., Cilibrasi, M., & Mayer, L. 2018, ApJL, 868, L13
Tang, Y. K., & Gai, N. 2011, A&A, 526, A35
van Werkhoven, T. I. M., Kenworthy, M. A., & Mamajek, E. E. 2014, MNRAS, 441, 2845
Vanderburg, A., Becker, J. C., Kristiansen, M. H., et al. 2016, ApJL, 827, L10
Waite, J. H., Perryman, R. S., Perry, M. E., et al. 2018, Sci, 362, aat2382
Wang, X., Li, L., Jiang, X., et al. 2024, NatCo, 15, 5045
Wisdom, J., Dbouk, R., Militzer, B., et al. 2022, Sci, 377, 1285
Ygouf, M., Beichman, C. A., Llop-Sayson, J., et al. 2024, AJ, 167, 26